Dispersion Distance and the Matter Distribution of the Universe in Dispersion Space

Kiyoshi Wesley Masui
Department of Physics and Astronomy, University of British Columbia, Vancouver, BC, Canada, V6T 1Z1 and Canadian Institute for Advanced Research, CIFAR Program in Cosmology and Gravity, Toronto, ON, Canada, M5G 1Z8

Kris Sigurdson
Department of Physics and Astronomy, University of British Columbia, Vancouver, BC, Canada, V6T 1Z1

We propose that 'standard pings', brief broadband radio impulses, can be used to study the three-dimensional clustering of matter in the Universe even in the absence of redshift information. The dispersion of radio waves as they travel through the Universe, like redshift, can be used as a cosmological distance measure. Due to inhomogeneities in the electron density along the line-of-siight dispersion is an imperfect proxy for radial distance and we show that this leads to calculable dispersion-space distortions in the apparent clustering of sources. Fast radio bursts (FRBs) are a new class of radio transients that are the prototypical standard ping, and due to their high observed dispersion from intervening plasma, have been interpreted as originating at cosmological distances. The rate of fast radio bursts has been estimated to be several thousand over the whole sky per day, and if cosmological, the sources of these events should trace the large-scale structure of the Universe. We calculate the dispersion-space power spectra for a simple model where electrons and FRBs are biased tracers of the large-scale-structure of the Universe and show that the clustering signal may be detectable in a survey with as few as 10000 events. Upcoming wide-field radio telescopes, like the Canadian Hydrogen Intensity Mapping Experiment (CHIME), are expected to detect...

Introduction—The clustering of matter on large scales has been heralded as the next great probe of the Universe after the cosmic microwave background (CMB). The large-scale structure in principle contains far more information than the CMB because it can be studied in three dimensions. Traditionally the redshift of spectral lines, caused by the Hubble flow, has been employed to measure radial distance and provide the third dimension. Such redshift surveys have now aggregated the positions of millions of galaxies into three dimensional density maps, exposing a rich structure of clusters, filaments, walls and voids.

However, redshift is not the only measure of radial distance. Standard candles and standard rulers can be used to estimate distance using brightness and angular size respectively. In the same way a *standard ping*, a brief broadband radio impulse, can be used to estimate radial distance because of the characteristic λ^2 dispersion of electromagnetic signals along the line-of-sight as a function of wavelength. This technique, widely used as an approximate distance indicator to pulsars in the Galaxy, can be used to define the *dispersion distance* to cosmological sources.

due to intervening plasma is readily measured from fast radio bursts (FRB) which are a class of radio transient first reported by **?**]. There have since been 10 such bursts reported [**?** **?** **?** **?** **?** **?**] and total rate of bursts been estimated to be $3.3^{+5}_{-2.5} \times 10^3$ per sky per day [**?**]. The dispersion measure (DM) is a line-of-site integral of the free electron density and can thus be used as a distance estimate, as is routinely done with galactic pulsars. FRB events are observed to have dispersion measures of order $1000\,\mathrm{pc/cm^3}$, greatly in excess of the galactic expectation of order $100\,\mathrm{pc/cm^3}$, depending on galactic latitude [**?**]. They must therefore be of extragalactic origin, with their dispersion produced either by the inter-galactic medium (IGM) [**?**] or the environment of the source [**?** **?** **?**]. If the dispersion is dominated by the intergalactic medium, then the average DM–distance relation can be modelled [**?** **?** **?**] and the sources are at cosmological distances of a few gigaparsecs. This would permit the study of the clustering of FRB sources in three dimensions which should trace the large-scale structure of the Universe on linear scales. Note that although we frame our discussions in terms of FRBs, dispersion may be

Neither redshift nor dispersion measure are perfect proxies for radial distance. Redshifts are systematically biased by the peculiar velocities of the object relative to the Hubble flow. This leads to additional apparent clustering in redshift space which was first calculated by **?**] using linear theory. Similarly, distance estimates from dispersion measure will be biased by inhomogeneities in the electron density [**?**], again leading to additional apparent clustering of sources in dispersion measure space. In this letter we calculate these DM-space distortions and consider the detectability of the signal by upcoming surveys.

Clustering in dispersion measure space—The dispersion measure of a signal observed in some angular direction $\hat{n}$ and originating from comoving radial distance χ is

$$\mathrm{DM}(\hat{n}, \chi) = \int_0^\chi \mathrm{d}\chi' a(\chi)^2 n_e(\hat{n}\chi', \chi'). \qquad (1)$$

Here $n_e(\vec{x}, \chi)$ is the free electron density as a function of location and conformal time. Note that we use χ as our radial distance and time coordinate, as opposed to redshift which is more appropriate for spectroscopic applications. We model the cosmological electron density as containing a homogeneous part and perturbations, $n_e(\vec{x}, \chi) = \bar{n}_e(\chi)\,[1 + \delta_e(\vec{x}, \chi)]$. The dispersion measure is thus

$$\mathrm{DM}(\hat{n}, \chi) = \int_0^\chi \mathrm{d}\chi' a(\chi')^2 \bar{n}_e(\chi')\,[1 + \delta_e(\hat{n}\chi', \chi')]\,. \qquad (2)$$

Dispersion measure space is the three dimensional coordinates, $\vec{x}_s$ inferred from the dispersion measure assuming that the electrons are homogeneous. This only affects the radial coordinate such that $\vec{x}_s = \hat{n}\chi_s$ with χ_s defined by the equation

$$\mathrm{DM}(\chi_s) = \int_0^{\chi_s} \mathrm{d}\chi' a(\chi')^2 \bar{n}_e(\chi'). \tag{3}$$

Combining the above equations (keeping only terms first order in the density perturbations), we find that

$$\frac{\mathrm{d}\chi_s}{\mathrm{d}\chi} = 1 + \delta_e(\hat{n}\chi, \chi), \tag{4}$$

and thus

$$\chi_s - \chi = \int_0^{\chi} \mathrm{d}\chi' \delta_e(\hat{n}\chi'). \tag{5}$$

We wish to relate the density of a tracer, f, measured in DM space to its density in real space. We follow the derivation in **?**] of the redshift-space distortions. Start by noting that the total number of tracers in a volume element is the same in both spaces:

$$n_{fs}(\vec{x}_s)\,\mathrm{d}^3\vec{x}_s = n_f(\vec{x})\,\mathrm{d}^3\vec{x}. \tag{6}$$

We split the density into a homogeneous part plus perturbations,

$$\bar{n}_{fs}(\chi_s)\left[1 + \delta_{fs}(\vec{x}_s)\right]\,\mathrm{d}^3\vec{x}_s = \bar{n}_f(\chi)\left[1 + \delta_f(\vec{x})\right]\,\mathrm{d}^3\vec{x}. \tag{7}$$

Averaged over the sky, $\langle\chi_s\rangle = \chi$ and thus the background density should be the same in DM space as in real space,

$$\bar{n}_{fs}(\chi) = \bar{n}_f(\chi). \tag{8}$$

Therefore,

$$\bar{n}_{fs}(\chi_s) = \bar{n}_f(\chi) + (\chi_s - \chi)\frac{\mathrm{d}\bar{n}_f}{\mathrm{d}\chi} \tag{9}$$

$$= \bar{n}_f(\chi) + \frac{\mathrm{d}\bar{n}_f}{\mathrm{d}\chi}\int_0^{\chi} \mathrm{d}\chi' \delta_e(\hat{n}\chi'). \tag{10}$$

The Jacobian in spherical coordinates is

$$\left|\frac{\mathrm{d}^3\vec{x}}{\mathrm{d}^3\vec{x}_s}\right| = \frac{\mathrm{d}\chi}{\mathrm{d}\chi_s}\frac{\chi^2}{\chi_s^2} \tag{11}$$

$$= (1+\delta_e)^{-1}\left(1 + \frac{\int_0^{\chi}\mathrm{d}\chi'\delta_e(\hat{n}\chi')}{\chi}\right)^{-2} \tag{12}$$

$$\approx 1 - \delta_e - \frac{2}{\chi}\int_0^{\chi}\mathrm{d}\chi'\delta_e(\hat{n}\chi'). \tag{13}$$

Substituting Equations 10 and 13 into Equation 6, we obtain

$$\delta_{fs} = \delta_f - \delta_e - \left(\frac{1}{\bar{n}_f}\frac{\mathrm{d}\bar{n}_f}{\mathrm{d}\chi} + \frac{2}{\chi}\right)\int_0^{\chi}\mathrm{d}\chi'\delta_e(\hat{n}\chi'). \tag{14}$$

In the equation above, the $-\delta_e$ term is most analogous to the Kaiser redshift-space distortions. It is a dilution of tracers in DM space due to an excess of electrons between the tracers. However we note that this term is isotropic in contrast to Kaiser. This is because any wave vector electron perturbation causes DM space distortions, whereas the radial velocities that cause redshift-space distortions are only sourced by perturbations with radial wave vectors.

The $\frac{1}{\bar{n}_f}\frac{\mathrm{d}\bar{n}_f}{\mathrm{d}\chi}$ arise since the misinterpretation of the radial distance causes the observed tracer density to be compared to the wrong background density. The $\frac{2}{\chi}$ term is caused by a misinterpretation of angular distances when the radial distance is mis-measured. In both cases analogous terms are in principle present in redshift space but are negligible. Because radial velocities are only sourced by modes with large radial wave vector, there is near perfect cancellation along the line of sight and thus is very little net error in radial distance.

For brevity in the following sections we define the coefficient of the integral term as

$$A(\chi) \equiv \frac{1}{\bar{n}_f}\frac{\mathrm{d}\bar{n}_f}{\mathrm{d}\chi} + \frac{2}{\chi}. \tag{15}$$

Large-scale structure is usually studied through its two-point statistics, most commonly the power spectrum, $P(k)$. Unlike in redshift-space distortions, Equation 14 does not have a simple form in harmonic space. The equation's third term couples harmonic modes and thus the two-point statistics cannot be phrased as a simple power spectrum. We will instead use $C_\ell^{ss}(\chi,\chi')$, which is the cross-correlation angular power spectrum of the DM-space over density, on shells at χ and χ':

$$\delta_{\ell\ell'}\delta_{mm'}C_\ell^{ss}(\chi,\chi') = \left\langle \int \mathrm{d}\Omega Y_{\ell m}(\hat{n})\delta_{fs}(\hat{n}\chi,\chi)\int \mathrm{d}\Omega' Y_{\ell' m'}(\hat{n}')\delta_{fs}(\hat{n}'\chi',\chi')\right\rangle. \tag{16}$$

The first two terms in Equation 14 are stationary. For stationary, isotropic, tracers x and y we have $\langle\delta_x(\vec{k},\chi)\delta_y(\vec{k}',\chi)\rangle = (2\pi)^3\delta^3(\vec{k}-\vec{k}')P_{xy}(k,\chi)$. If for a moment we ignore time dependence, the angular cross-power spectrum of such tracers is

$$C_\ell^{xy}(\chi,\chi') = \frac{2}{\pi}\int_0^{\infty}\mathrm{d}k k^2 j_\ell(k\chi)j_\ell(k\chi')P_{xy}(k). \tag{17}$$

In reality the power spectrum evolves on the order of a Hubble time. The angular cross correlations will be very small unless χ and χ' are within a few correlation lengths of one another, roughly a hundred megaparsecs. The evolution of the power-spectrum is negligible over these time differences which leads to a straight-forward way to include the evolution of the perturbations:

$$C_\ell^{xy}(\chi,\chi') \approx \frac{2}{\pi}\int_0^{\infty}\mathrm{d}k k^2 j_\ell(k\chi)j_\ell(k\chi')P_{xy}(k,(\chi+\chi')/2), \quad |\chi-\chi'| \ll 1/aH. \tag{18}$$

The third term in Equation 14 is not stationary but is an integral over the stationary field δ_e. Define δ_d as

$$\delta_d(\hat{n}\chi) \equiv \int_0^{\chi} \mathrm{d}\chi' \delta_e(\hat{n}\chi'). \tag{19}$$

It is straight-forward to show that

$$C_\ell^{dd}(\chi,\chi') = \frac{2}{\pi}\int_0^{\chi} \mathrm{d}\chi'' \int_0^{\chi'} \mathrm{d}\chi''' \int_0^{\infty} \mathrm{d}k k^2 j_\ell(k\chi'') j_\ell(k\chi''') P_{ee}(k,(\chi''+\chi''')/2). \tag{20}$$

Finally, C_ℓ^{ss} will contain cross terms between the stationary terms and the integral terms. These will have the form

$$C_\ell^{dx}(\chi,\chi') = \frac{2}{\pi}\int_0^{\chi} \mathrm{d}\chi'' \int_0^{\infty} \mathrm{d}k k^2 j_\ell(k\chi') j_\ell(k\chi'') P_{ex}(k,(\chi'+\chi'')/2). \tag{21}$$

Assembling all these expressions with the proper coefficients we have

$$\begin{aligned} C_\ell^{ss}(\chi,\chi') = & \frac{2}{\pi}\int_0^{\infty} \mathrm{d}k k^2 j_\ell(k\chi) j_\ell(k\chi') P_{[ff+ee-2ef]}(k,(\chi+\chi')/2) \\ & + \frac{2}{\pi}A(\chi)A(\chi')\int_0^{\chi} \mathrm{d}\chi'' \int_0^{\chi'} \mathrm{d}\chi''' \int_0^{\infty} \mathrm{d}k k^2 j_\ell(k\chi'') j_\ell(k\chi''') P_{ee}(k,(\chi''+\chi''')/2) \\ & + \frac{2}{\pi}A(\chi)\int_0^{\chi} \mathrm{d}\chi'' \int_0^{\infty} \mathrm{d}k k^2 j_\ell(k\chi') j_\ell(k\chi'') P_{[ee-fe]}(k,(\chi'+\chi'')/2) \\ & + \frac{2}{\pi}A(\chi')\int_0^{\chi'} \mathrm{d}\chi'' \int_0^{\infty} \mathrm{d}k k^2 j_\ell(k\chi) j_\ell(k\chi'') P_{[ee-fe]}(k,(\chi+\chi'')/2). \end{aligned} \tag{22}$$

Here, expressions such as $P_{[ff+ee-2ef]}$ are short hand for $P_{ff} + P_{ee} - 2P_{ef}$.

Equation 22 can be simplified substantially by adopting the small angle and Limber approximations [**? ? ?**]. The small angle approximation eliminates the k integral over spherical Bessel functions, replacing it with a Fourier transform, and is valid for $\ell \gg 1$. The Limber approximation assumes that only modes with small radial component of their wave vector contribute to the radial integrals and is valid if the power spectra evolve slowly compared to the correlation length [**?**] (which has already been assumed). With these approximations we have

$$\begin{aligned} & C_\ell^{ss}(\chi,\chi') \approx \\ & \frac{1}{\bar{\chi}^2}\int_{-\infty}^{\infty} \frac{\mathrm{d}k_\parallel}{(2\pi)} e^{ik_\parallel(\chi-\chi')} P_{[ee+ff-2ef]}(\sqrt{k_\parallel^2+\nu^2/\bar{\chi}^2},\bar{\chi}) \\ & + A(\chi)A(\chi')\int_0^{\chi_{\min}} \mathrm{d}\chi'' \frac{1}{\chi''^2} P_{ee}(\nu/\chi'',\chi'') \\ & + \frac{A(\chi_{\max})}{\chi_{\min}^2} P_{[ee-ef]}(\nu/\chi_{\min},\chi_{\min}), \end{aligned} \tag{23}$$

where $\nu \equiv \ell + 1/2$, $\chi_{\min} \equiv \min(\chi,\chi')$, and $\chi_{\max} \equiv \max(\chi,\chi')$. We've found that these approximations are excellent for $\ell \gtrsim 10$ and use this form for the remainder of the paper. In the above equation we dub the three terms the 'local', 'integral' and 'cross' terms respectively and will refer to them as such henceforth.

Modelling and measurement—There are a number of effects that will complicate the measurement of the above calculated angular power spectrum by a real survey of dispersion measures. The first effect is that the model that the free electron density decomposes into a homogeneous part plus a random field of perturbations is not complete. Firstly, all signals must pass through the Milky Way's galactic disk, halo, and local environment, which will contribute to the dispersion measure. However, this is only a single function of $\hat{n}$ which can presumably be well measured. In addition, this function could in principle be well characterized by independent data such as observations of pulsars. As such, it should be possible to subtract the local contribution, as was done in **?**], and this is unlikely to be a limiting obstacle.

More concerning is the dispersion from the source's environment as well as the halo in which it resides. These electrons will presumably be clustered around the source on scales far smaller than DM-space structure map pixels and thus are not accounted for in the δ_e–δ_f correlations included in the above formalism. This will have a mean contribution, common to all sources and which may be epoch dependant, that will modify the mean DM–distance relation. This will need to be calibrated in some why or else fit with nuisance parameters during parameter estimation. There will also be a stochastic piece which varies from source to source. This will limit the precision at which χ_s can be measured, thus limiting the resolution of DM space density maps in the radial direction.

Detailed treatment of the above complications is beyond the

scope of this work. The magnitude of the contribution from the progenitor is at present unknown. To crudely deal with it here we use relatively large χ bins of $100\,\mathrm{Mpc}/h$ in sensitivity estimates.

The second term in Equation 23 is an integral that mixes many spatial scales: small scales from smaller radial distance and larger scales from greater distances. The mixing of scales complicates the interpretation of measurements, since structure formation on scales smaller than $\sim 10\,\mathrm{Mpc}/h$ is non-linear and hard to model. A similar issue exists in the field of weak gravitational lensing, where the formula for the angular power spectrum has a similar form. In lensing, a kernel in the line-of-sight integral arising from geometric effects suppresses the contribution from small distances, partially alleviating the issue.

There is an advantage to the lack of kernel in the DM-space integral term. Lensing tomography—the use of sources at multiple redshifts to un-mix spatial scales—is complicated by the kernel. The kernel's shape depends on the source redshift, re-weighting the line-of-sight integral and making tomography inexact. In contrast the integrand in the DM-space integral term is completely independent of the limit of integration, meaning contributions from different parts of the line of sight (and thus different spatial scales) can be separated exactly. Again, a detailed study of DM space tomography is beyond the scope of this work. To avoid our results being sensitive to the hard-to-model small scales, we assume that the contribution to the integral term from radial distances $\chi'' < 500\,\mathrm{Mpc}/h$ are well measured by the correlations with these radial slices. We thus neglect the information from these slices in our sensitivity measurements and ignore contributions to the integral term from below this distance. The smallest spatial scale that contributes the our plotted angular power spectra out to $\ell = 1000$ is thus $k = 2\,h/\mathrm{Mpc}$.

For plotting the DM-space power spectra we use a toy model for the electron and FRB clustering that assumes both are biased tracers of the dark matter: *i.e.* $P_{xy}(k) = b_x b_y P(k)$. We calculate the time dependant dark-matter power spectrum using `CAMB` using the integrated `HALOFIT` to approximate the non-linear evolution. We assume that the electron bias is $b_e = 1$, which should be true on large scales due to the approximate conservation of free electrons. The bias of FRB sources is unconstrained by data and we choose it to be $b_f = 1.3$. The coefficient $A(\chi)$ depends on the density of detected FRB sources, $\bar{n}_f(\chi)$. We use a simple model where all events above a fixed flux are detected, the intrinsic luminosity function has the **?**] form with index -1, and events at the cut off of the luminosity function and at a radial distance of $\chi = 2350\,\mathrm{Mpc}/h$ are at the flux detection threshold. This source density is shown in Figure 1 with the resulting DM-space power-spectrum in Figure 2.

In first measurements of the angular power spectra, uncertainty will be dominated by the finite number of observed dispersion measures, or shot noise. The noise power spectrum on

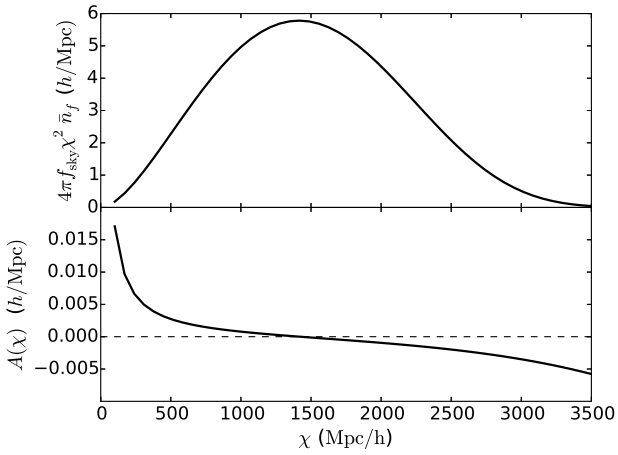

FIG. 1. *Top:* Comoving density of sources in toy model, as described in text. Normalization is such that the survey has a total of 10^4 FRB events. *Bottom:* Resulting coefficient $A(\chi)$ as given in Equation 15.

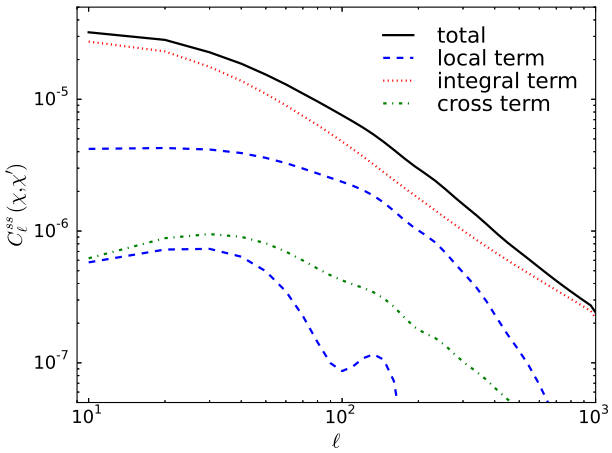

FIG. 2. Terms in the DM-space cross-correlation angular power spectrum. All terms are evaluated at $\bar{\chi} = 2000\,\mathrm{Mpc}/h$ and $\chi - \chi' = 10\,\mathrm{Mpc}/h$, except the lowest most "local term" curve which is for $\chi - \chi' = 50\,\mathrm{Mpc}/h$. While the other two terms are highly insensitive to the separation of the radial slices, the local term drops rapidly with separation.

shells with of width $\Delta\chi$ is

$$C^N_{\ell,ij} = \frac{\delta_{ij}}{\bar{n}_f(\chi_i)\chi_i^2\Delta\chi}. \tag{24}$$

Here, to indicate that we are now working with quantities binned in the radial direction instead of continuous functions, we've switched to $C_{\ell,ij}$ over $C_\ell(\chi,\chi')$. The uncertainty on the angular cross-power spectrum is then

$$(\Delta C^{ss}_{\ell,ij})^2 = \frac{1}{\ell(\ell+1)\Delta\ell f_{\rm sky}}\left[C^N_{\ell,ii}C^N_{\ell,jj} + (C^N_{\ell,ij})^2\right], \tag{25}$$

where the second term in brackets only contributes for $i = j$.

We consider the sensitivity of a survey with a total of 10^4 dispersion measures from FRB events distributed uniformly

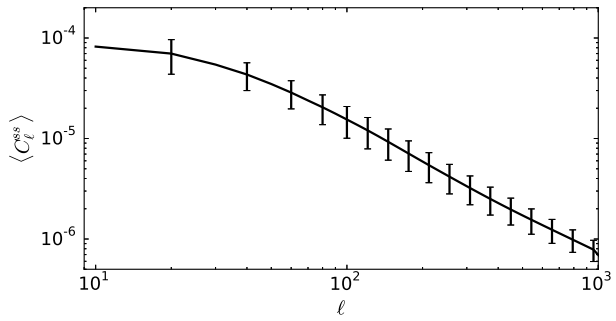

FIG. 3. Sensitivity of a survey with 10^4 dispersion measures distributed uniformly over half the sky. Plotted is the cross-correlation power spectrum weighted averaged over all pairs of radial bins. Weights are chosen to maximize signal to noise at $\ell = 100$.

over half the sky. This is in rough approximation to what could be achieved by the Canadian Hydrogen Intensity Mapping Experiment's now funded FRB instrument over a three year survey. To give an idea of the overall sensitivity of the survey, we collapse $C^{ss}_{\ell,ij}$ to a single function of ℓ by taking a weighted average of all pairs of radial bins. We use bin widths of $100\,\mathrm{Mpc}/h$ over the range $500\,\mathrm{Mpc}/h$ to $3500\,\mathrm{Mpc}/h$. For weights in the radial bin average, we use the signal over noise-squared at $\ell = 100$, which maximizes the signal to noise at that ℓ and is near optimal at other multipoles. We exclude the $i = j$ bin pairs as they would be contaminated by noise bias in a real survey. This effectively discards the contribution from the local term. The result is shown in Figure 3.

Discussion and conclusions—We have proposed using FRB sources as 3D tracers of the large-scale structure, using dispersion measure to estimate radial distance. It can be seen in Figure 2 that the signal is dominated by inhomogeneities in the electron density along the line of sight inducing mis-estimates of radial distance and thus apparent clustering. These DM-space distortions could be used to study the distribution of free electrons in the Universe on large-scales. There have been other proposals to use FRB events to study large-scale structure [**? ?**], however these schemes have either been two dimensional or required externally measured redshifts for the sources. Additionally, there have been proposals to use the DM-redshift relation to probe the background density of electrons and thus the expansion history of the Universe [**? ? ?**].

We have shown that a survey detecting 10^4 fast radio bursts of cosmological origin (as might be achieved by the CHIME FRB instrument) could detect the clustering signal. Looking forward, DM-space clustering could become a powerful probe of large-scale structure should observational factors turn out to be favourable compared to spectroscopic surveys. The baryon acoustic oscillation feature can be clearly seen in Figure 2 in the cross term and both local-term curves. It may also be possible to extract the BAO feature from the integral term using tomography. This however requires that the contribution to dispersion measure from the source's environment and host halo be modest compared to the contribution from the IGM.

We thank Ue-Li Pen and Mathew McQuinn for helpful discussions. KWM is supported by the Canadian Institute for Advanced Research, Global Scalars Program.